New search for the neutron electric dipole moment with ultracold neutrons at ILL

A. P. Serebrov,* E. A. Kolomenskiy, A. N. Pirozhkov, I. A. Krasnoschekova, A. V. Vassiljev, A. O. Polyushkin, M. S. Lasakov, A. N. Murashkin, V. A. Solovey, A. K. Fomin, I. V. Shoka, and O. M. Zherebtsov
B. P. Konstantinov Petersburg Nuclear Physics Institute of National Research Centre "Kurchatov Institute," 188300 Gatchina, Leningrad region, Russia

P. Geltenbort, S. N. Ivanov, and O. Zimmer
Institut Max von Laue – Paul Langevin, BP 156, 38042 Grenoble Cedex 9, France

E. B. Alexandrov, S. P. Dmitriev, and N. A. Dovator
Ioffe Physical Technical Institute RAS, 194021 St. Petersburg, Russia
(Received 16 February 2015; revised manuscript received 29 July 2015; published 5 November 2015)

The search for an electric dipole moment (EDM) of the neutron is a crucial test for theoretical particle physics models with violation of time and spatial invariance. A new experiment recently has been carried out at the High-Flux Reactor at Institut Laue-Langevin, using the upgraded double-chamber magnetic resonance spectrometer developed at Petersburg Nuclear Physics Institute. The result is interpreted as an upper limit on the value of the neutron EDM, $|d_n| < 5.5 \times 10^{-26} e$ cm (90% C.L.). This article provides a detailed description of the setup and experimental procedures, along with a discussion of possibilities for further improvement of the experimental accuracy.

DOI: 10.1103/PhysRevC.92.055501 PACS number(s): 14.20.Dh, 29.90.+r

I. INTRODUCTION

Symmetry is one of the key concepts in modern physics. Invariance of elementary processes under symmetry transformations implies a certain character of the physical laws. One of the fundamental theorems of the quantum field theory is the CPT theorem, according to which all physical interactions are invariant with respect to combined CPT transformation, where C, P, and T are the discrete symmetry transformations of charge conjugation, space reflection (parity), and time reversal, respectively. Elementary particles can possess an electric dipole moment (EDM) only in case of simultaneous violation of P and T symmetries.

As far back as 1950 Purcell and Ramsey pointed out that "the validity of the parity assumption must rest on experimental evidence" [1,2]. A few years later, information on the first experimental search for a neutron EDM became available. Interest in this problem has considerably grown after discovery of parity violation in the weak interaction [3,4] and notably of CP-invariance violation in the decays of neutral K mesons [5]. In the macro world indirect evidence for processes involving violation of CP invariance is the baryon-antibaryon asymmetry observed in our universe. Understanding the character of fundamental symmetry violations is supposed to shed light on the origin and evolution of the universe at its very first stages.

The standard model (SM) of electroweak interactions, which describes the CP violation observed in processes with K and B mesons by a single complex parameter [a phase in the Cabibbo-Kobayashi-Maskawa (CKM) quark-mixing matrix] provides estimates of the neutron EDM value on the level $\sim 10^{-32}\, e$ cm, inaccessible for any experiment using currently known techniques. However, the CP violation in the SM predicts a value of only $\sim 10^{-20}$ for the baryon-antibaryon asymmetry in the universe, which is way too small to ever become reconciled with observed value of 6×10^{-10} (see, e.g., Refs. [6,7]). Therefore, a mechanism of CP violation beyond the SM has to exist.

Theories beyond the SM, such as supersymmetry, multi-Higgs models, or left-right symmetric models, provide much larger values for the neutron EDM at the level $10^{-26} - 10^{-28}\, e$ cm [8,9]. A possibility to generate the baryon-antibaryon asymmetry at the observed level is known as electroweak baryogenesis. It requires new physics that can be discovered both in searches of rare processes at the Large Hadron Collider and in searches of permanent dipole moments of the neutron, the electron, and neutral atoms. Both the high-energy and low-energy experiments are important complements, and even the EDM searches of different species complement each other due to sensitivity to different mechanisms of CP violation [10–12].

While the latest measurement on the electron EDM [13] challenge the minimal supersymmetric model of the electroweak baryogenesis [14,15], further enhancement of sensitivity in searches for EDMs of other elementary particles such as the neutron will help to resolve possible non-SM CP-violation mechanisms [10–12]. For illustration, Fig. 1 shows areas of mass parameters [supersymmetric Higgs-Higgsino mass versus the $U(1)_Y$ gaugino mass parameter M_1] of a specific supersymmetric model already excluded by other experiments [14]. The dash-dotted line shows the sensitivity to the neutron EDM, which might become accessible using new ultracold neutron (UCN) sources of high intensity.

The first experiments to search for a neutron EDM were based on a magnetic resonance beam method suggested by

*serebrov@pnpi.spb.ru

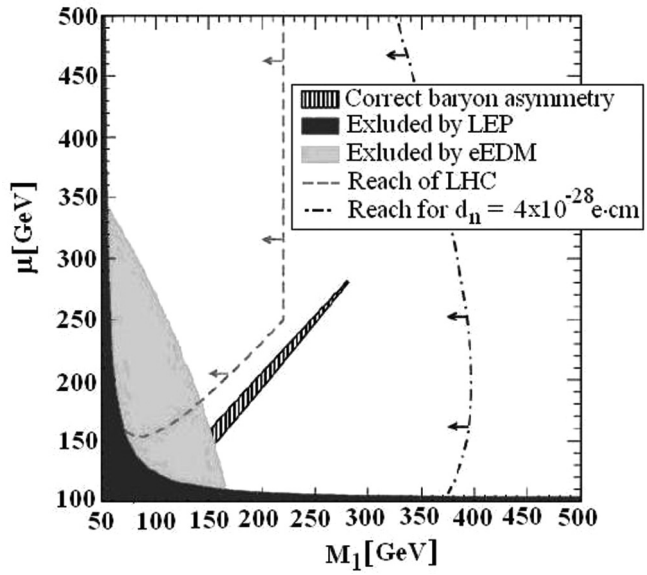

FIG. 1. Sensitivity of present and future EDM measurements to the mass parameters of an exemplary supersymmetric model relevant for discussion of the electroweak baryon genesis (from Ref. [14]).

N. Ramsey [2,16]. An alternative possibility to detect it in a scattering experiment was proposed by C. Shull and R. Nathans [17]. There, the neutron interacts with the atomic Coulomb field, which is much stronger than any electric field achievable in laboratory.

The main difficulty of experiments using beams of thermal or cold neutrons is the suppression of systematic effects mimicking a neutron EDM. Here, a major source of uncertainty is the interaction of the neutron magnetic moment with the magnetic field seen by the neutron moving in the electric field (called the "$\mathbf{v} \times \mathbf{E}$ effect"). The accuracy of early experiments was limited due to systematic uncertainties rather than counting statistics. The latest Ramsey-type beam experiment provided a best constraint on the neutron EDM of $|d_n| < 3 \times 10^{-24}\, e$ cm [16].

A different class of experiments involves neutron scattering in a non-centro-symmetric crystal as developed by a group from Petersburg Nuclear Physics Institute (PNPI) [18,19]. Here neutrons interact with very strong atomic electric fields and the interaction time is in the order of a second due to Bragg's angles close to $\pi/2$. The result of a first measurement is $d_n = (2.5 \pm 6.5^{\text{stat}} \pm 5.5^{\text{syst}}) \times 10^{-24}\, e$ cm [20]. The authors believe that, using an upgraded setup, they can improve the statistical uncertainty down to $10^{-26}\, e$ cm.

The use of ultracold neutrons for investigation of neutron properties has opened up new experimental possibilities. Ya. B. Zel'dovich first pointed out the possibility to store neutrons with low kinetic energy in a closed vessel [21]. Trapping occurs if the kinetic energy of neutrons is less than the neutron optical potential of wall materials, so neutrons will be reflected under any angle of incidence. The proposal to use UCN to search for an electric dipole moment of the neutron was put forward by F. L. Shapiro [22]. The first experimental evidence for UCN extracted from a reactor was provided at JINR in Dubna [23] and at TU Munich in Garching [24]. Shortly afterwards, work with ultracold neutrons was also started at the PNPI WWR-M reactor under the guidance of V. M. Lobashev. His team created UCN sources of high intensity and the first polarized UCN beams and gave a proof of principle for using UCN in the neutron EDM search.

A first publication of a neutron EDM experiment using UCN at PNPI dates back to the early 1980s [25]. As early as 1981 the first constraint, $|d_n| < 1.6 \times 10^{-24}\, e$ cm (90% C.L.), was improved to $|d_n| < 6 \times 10^{-25}\, e$ cm (90% C.L.) [26]. Complemented with activities of a collaboration of Rutherford Appleton Laboratory (RAL), Sussex University, and the Institut Laue-Langevin (ILL) [27,28], an EDM limit of $\sim 1 \times 10^{-25}\, e$ cm (90% C.L.) was established early in the 1990s [29–31]. Measurements in Gatchina (Russia) were then stopped due to failure of the UCN source. Continuation of measurements in Grenoble over 15 years further improved the upper limit on the neutron EDM by a factor 3 [32]. Still today, the result $|d_n| < 2.9 \times 10^{-26}\, e$ cm (90% C.L.) represents the best constraint ever obtained. The experiment employed a single chamber for storing UCN together with mercury atoms as a comagnetometer. This scheme for monitoring the magnetic field was found susceptible to a species-dependent geometric phase effect, requiring special care to keep it under control [33].

While our current work has not yet reached the same level of precision as the result given in Ref. [32], it employs a different experimental approach. Indeed, we use a differential magnetoresonance spectrometer composed of a double chamber for storing UCN, with a common constant magnetic field and electric fields of opposite directions in the chambers. As discussed below, this setup offers experimental control over possible false effects. Note that, in the measurements presented here, we have not found systematic errors at the established level of precision.

Figure 2 shows the chronology of experimental results. Latest measurements conducted in Gatchina employed the UCN source described in Ref. [34] while measurements at ILL in Grenoble since 1986 use neutrons from the public user source PF2, comprising a neutron turbine coupled to a

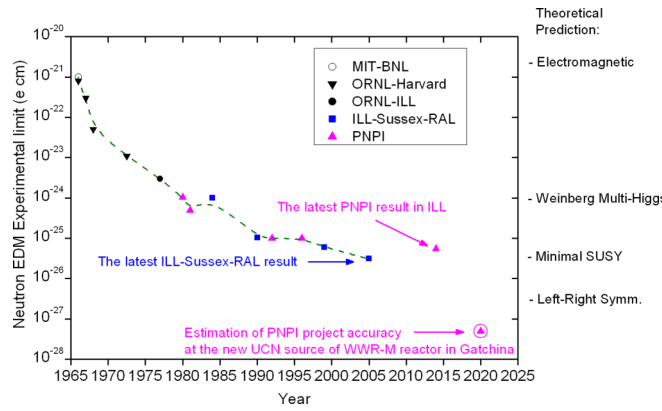

FIG. 2. (Color online) Chronology of experimental upper limits on the neutron EDM and a perspective for an increase of precision.

liquid-deuterium cold source via a vertical guide for very cold neutrons [35].

Currently, most groups focus on using UCN to conduct neutron EDM experiments with improved sensitivity [36–41]. A notable exception is the proposed in-beam experiment described in Ref. [42]. An experiment with UCN involving a fully cryogenic setup described in Ref. [43] has recently been discontinued. An advantage of storing UCN in closed vessels is a long interaction time of the neutron with applied magnetic and electric fields, along with mitigation of the aforementioned $\mathbf{v} \times \mathbf{E}$ effect due to low neutron velocity and directional changes of UCN motion after each wall collision. The final experimental accuracy of our installation has mainly been limited by the number of counted neutrons. Hence, perspectives for sensitivity increase of EDM experiments are intimately linked to the availability of a novel generation of UCN sources.

With this strong motivation, many laboratories around the globe are developing such sources. Progress has been reported from ILL (France) [44,45], Los Alamos National Laboratory (USA) [46], Paul Scherrer Institute (Switzerland) [47], Technische Universität München and Mainz (Germany) [48–53], and the Research Center for Nuclear Physics (Japan) [54,55]. A project at TRIUMF (Canada) will be based on the latter development of a superfluid-helium source closely coupled to a neutron spallation source. The project of a solid-deuterium UCN source at the PulSTAR reactor at North Carolina State University is close to being completed [56]. UCN source projects for the high flux reactor PIK under construction at PNPI and for the operating reactor WWR-M in Gatchina are based on superfluid helium [57,58]. The calculated UCN density in these sources (like in some of the aforementioned projects) is 2–3 orders higher than what is available at the beam ports of PF2 [59]. The corresponding leap in neutron-EDM sensitivity to a level better than $10^{-27}\ e$ cm, as illustrated in Fig. 2, will enable tests of hitherto inaccessible theoretical models of CP violation (supersymmetric, left-right symmetric, and others).

This work describes the double-chamber differential magnetoresonance EDM spectrometer manufactured at PNPI together with latest results from data taking at the beam line PF2/MAM at ILL's High Flux Reactor. A Letter has already been published in Ref. [36].

II. GENERAL PRINCIPLES OF EXPERIMENTAL METHOD

As a consequence of the Wigner-Eckart theorem, the neutron EDM vector $\mathbf{d}_n$, if existent, must be collinear to the neutron spin ($s = 1/2$). The energy of interaction of the neutron magnetic moment $\boldsymbol{\mu}$ with a constant and uniform magnetic field $\mathbf{B}_0$ is $W = -(\boldsymbol{\mu}\mathbf{B}_0)$, and the neutron energy state splits into two Zeeman sublevels corresponding to two possible projections of the neutron spin. For an electric field $\mathbf{E}$ applied collinear to $\mathbf{B}_0$, the neutron interaction with the fields is given by the Hamiltonian

$$W = -(\boldsymbol{\mu}\mathbf{B}_0) - (\mathbf{d}_n\mathbf{E}).$$

The term due to the small d_n induces a frequency shift of the magnetic resonance. If $\mathbf{E}$ and $\mathbf{B}_0$ are parallel and the neutron EDM is positive, $d_n > 0$, then magnetic resonance frequency decreases,

$$f = 2\mu B_0 h^{-1} - 2d_n E^+ h^{-1}.$$

Reversal of the electric field changes the frequency of spin precession by $\Delta f = 2d_n(E^+ + E^-)h^{-1}$. Hence,

$$d_n = \frac{\Delta f h}{2(E^+ + E^-)},$$

where E^+ and E^- are the strengths of the electric field for $\mathbf{E}$ parallel and antiparallel to $\mathbf{B}_0$, respectively, Δf is the frequency shift of the neutron spin precession, and h is Planck's constant.

Ramsey's method of separated oscillating fields is the most sensitive technique for registering a spin-precession frequency shift [60]. Employed for UCN storage, one applies two coherent radio frequency (rf) pulses of a magnetic field $\mathbf{B}_1$ perpendicular to $\mathbf{B}_0$ and with frequency f close to the neutron Larmor frequency $f_0 = 2\mu B_0 h^{-1}$ at the beginning and at the end of a neutron storage interval. Magnitude and duration of each $\mathbf{B}_1$ pulse are chosen such as to rotate the neutron polarization initially parallel to $\mathbf{B}_0$ by an angle $\pi/2$. Following the first rf pulse, during the storage time T the neutron spins precess freely about $\mathbf{B}_0$. For $f = f_0$, and without a relative phase between the two rf pulses, the final neutron polarization will be opposite to the initial one. For a 180° phase shift between pulses, the original polarization will be restored, while for 90° or 270° the neutron spins will remain in the plane perpendicular to $\mathbf{B}_0$. In this case the mean polarization along $\mathbf{B}_0$ will vanish, unless an additional phase will be accumulated during precession, e.g., due to the electric dipole moment interaction with an electric field. Neutron polarization analysis after the second rf pulse will make this phase visible. Figure 3 shows exemplary resonance curves measured with detectors attached to the two chambers as a function of rf

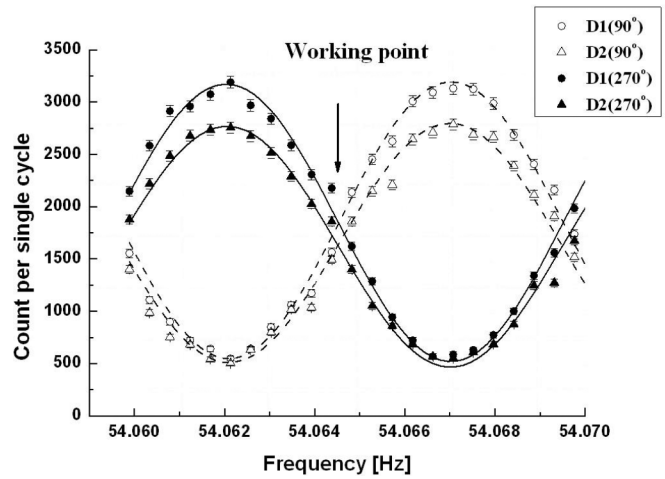

FIG. 3. Central parts of the Ramsey resonance curves measured using the detectors D1 and D2 connected to the two neutron chambers (see Fig. 4) and for phase shifts of 90° and 270° between the rf-pulses. The visibility of the resonance was about 0.7 for $T = 95$ s.

frequency f, for time interval $T = 95$ s between two rf pulses with a relative phase shift of 90° and 270°, respectively. In order to account for magnetic-field instabilities, frequency scanning is performed using a special electronic scheme to lock the ratio of applied frequency to average frequency of eight cesium magnetometers located around the UCN storage cells as discussed in detail in Sec. IIIC.

As visible in Fig. 3, the slope of resonance curves, i.e., the change of neutron counts with f, is highest at a resonance point where the curves for 90° and 270° relative phase shifts intersect. In the vicinity of this "working point" curves are well described as sinusoidal, i.e.,

$$N(f) = \alpha N_{\rm res} \sin[2\pi T(f - f_0)] + N_{\rm res},$$

where $\alpha = (N_{\rm max} - N_{\rm min})/(N_{\rm max} + N_{\rm min})$ is the visibility of the resonance curve, T is the time between pulses, and $N_{\rm res}$ is the number of counted neutrons at the resonance frequency. The longer is T, the narrower will be the resonance curve and the higher the sensitivity to a frequency shift Δf. The difference of counted neutrons for two cycles of storage for opposite directions of $\mathbf{E}$ can be expressed as

$$N^+ - N^- = \Delta f(\partial N/\partial f) = 2\pi \Delta f \alpha N_{\rm res} T,$$

where $\partial N/\partial f$ is the slope of the resonance curve taken at the working point, with the sign depending on the choice of the phase between the two rf pulses. We thus obtain the following expression for the neutron EDM:

$$d_n = \frac{h(N^+ - N^-)}{2(E^+ + E^-)\frac{\partial N}{\partial f}}, \quad (1)$$

with the statistical error expressed by

$$\delta d_n = \frac{h\sqrt{2N_{\rm res}}}{2(E^+ + E^-)\frac{\partial N}{\partial f}} = \frac{h\sqrt{2N_{\rm res}}}{2(E^+ + E^-)\alpha 2\pi T N_{\rm res}}, \quad (2)$$

with $2N_{\rm res} = N^+ + N^-$.

Summarizing, the experimental sensitivity is determined by neutron count numbers, the width and visibility of the resonance curve and the electric field strength. The slope of the resonance curve at the working point depends on both the initial polarization of neutrons and its preservation during storage. Inhomogeneity and fluctuations of the magnetic field and collisions with the trap walls may result in partial neutron depolarization, thus decreasing the sensitivity.

III. THE PNPI DIFFERENTIAL EDM SPECTROMETER

In the experiment described here we used an upgraded version of the double-chamber EDM spectrometer described in Ref. [30], including several major changes in the equipment:

(a) upgrade or renewal of all electronics;
(b) a new high voltage (HV) supply with modernized control scheme and system for measurement of leakage currents;
(c) a new magnetometry system based on the eight cesium magnetometers with frequency divider;
(d) first employment of sitall as insulator material in the neutron storage chambers;

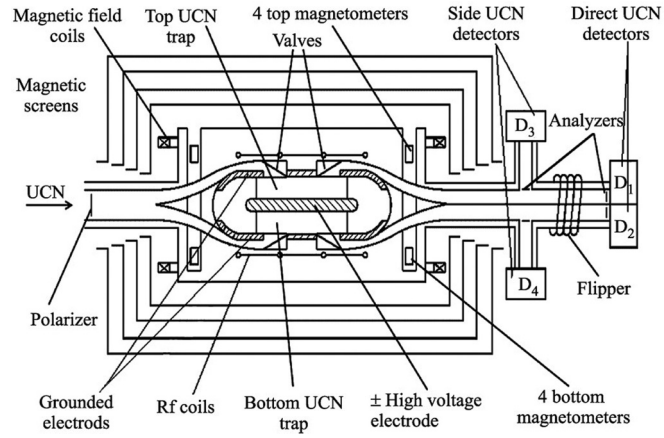

FIG. 4. Layout of the EDM spectrometer (vertical cut through the center).

(e) first coating of insulator rings with ^{58}Ni-oxide/molybdenum; and
(f) new software for experiment control and data acquisition.

The layout of the spectrometer and its implementation are shown in Figs. 4 and 5. A special feature is a double chamber for UCN storage in a common magnetic field. Electric fields applied in the chambers have equal magnitude but opposite direction. Changing the polarity of the electric fields inverts the neutron EDM effects in the chambers, whereas

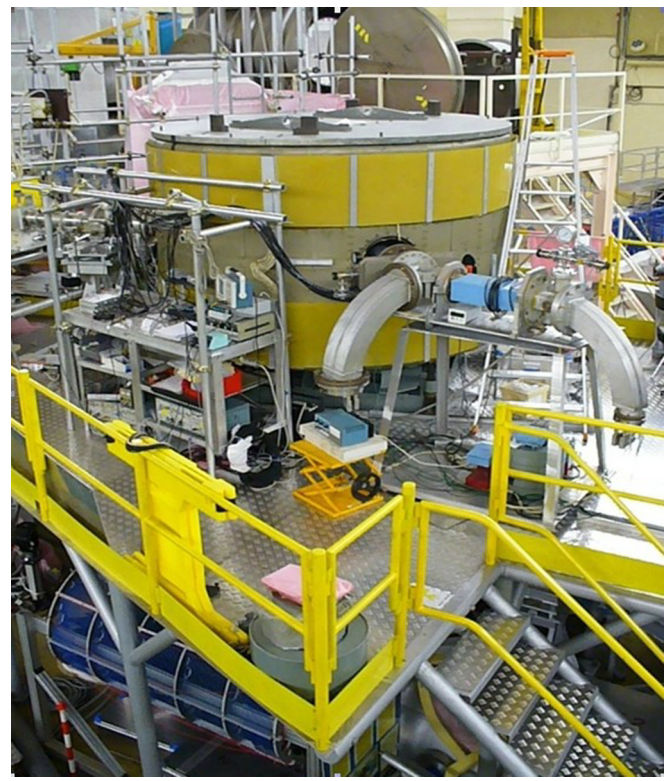

FIG. 5. (Color online) Photograph of the PNPI spectrometer implemented on its platform in the experimental hall of ILL.

any instability of the common electromagnetic conditions will shift the resonance frequency in both chambers in the same direction. Taking proper count rate differences will thus result in a strong suppression of non-neutron EDM effects.

In addition, the installation possesses a system of double polarization analysis. Every storage chamber is connected to two detectors, one for analysis of the component parallel to $\mathbf{B}_0$ and a second one equipped with a spin flipper located in front of the second analyzer for registering the opposite polarization component. This increases the total number of counted neutrons and allows us to compensate intensity fluctuations of the neutron source. As discussed further below, suitable combination of count rates from different detectors also provides a handle on systematic effects.

It should be noted that four detectors in the spectrometer do not have equal count rate. Due to different geometry of neutron guides, storage chamber location, properties of polarization analyzers we have an asymmetry in the UCN counts which slightly reduces the compensation mechanism and somewhat distorts the correlation analysis. Next, we give a short description of the basic units of the setup.

Neutron guides: Ultra cold neutrons are transported from the neutron turbine to the polarizer by a rectangular neutron guide with cross section $70 \times 60\,\mathrm{mm}^2$, made from stainless steel and coated with the isotope alloy ^{58}Ni(90%)Mo(10%) with a critical velocity for UCN about 7.8 m/s. The neutron guide behind the polarizer is made from nonmagnetic materials such as copper replica, obtained at glass, or nonmagnetic nickel-molybdenum alloy coated onto glass with high surface quality. This guide is divided to feed the storage chambers with neutrons through the outer electrodes.

Polarizer: Polarization and polarization analysis are performed outside the magnetic screens in the input and output neutron guides, respectively, by passing the UCN through foils, magnetized to saturation in the field of permanent magnets. These foils were made by sputtering a layer of 200 nm of Fe(55%)Co(45%) alloy onto a titanium substrate of 120 nm thickness. The neutron polarization after passage through the polarizer foil was ~90%.

Neutron detectors: Proportional ^{3}He counters with aluminum windows of 0.1 mm thickness were used. To reduce the neutron losses on the aluminum foils in front of the detectors, neutrons were accelerated by 0.6 m free fall in the gravitational field. The efficiency of neutron registration is 80%.

UCN storage chambers: They are located in the main aluminum vacuum vessel surrounded by the magnetic screens. All spectrometer units inside the magnetic shielding are made from nonmagnetic materials such as aluminum, titanium, beryllium bronze, Teflon, or glass. The vertical walls of the UCN storage chambers are formed by rings made from an insulating material with a large volume electric resistance, either quartz or glass ceramics, see discussion below. The height of the rings is about 100 mm, and the inner diameter is 526 mm. The inner surfaces of the isolator rings were sputter coated either with beryllium oxide or a compound of ^{58}Ni oxide and molybdenum, which both are good electric isolators and have a critical velocity of 6.8 m/s for UCN. The landing grooves of 6.5 mm depth are made in the electrodes to hold the rings in place and avoid high-voltage breakdowns at electrode-isolator contact points. The top and bottom lids of the neutron storage chambers are electrodes made from polished aluminum and coated with beryllium. They are equipped with shutters for filling and emptying the chambers with neutrons and always kept at zero potential with respect to the high voltage applied to the central electrode common to both chambers. Electrical contacts are made at the center of the electrodes. As discussed in more detail below, this provides a symmetrical distribution of magnetic fields generated by the leakage currents in the neutron storage chambers, thus reducing their impact on systematic. The spectrometer vacuum of $\sim 10^{-5}$ mbar was created by turbomolecular pumps.

Fused quartz and glass ceramics were used for the ring insulators. Glass ceramic is a microcrystalline material characterized by high hardness, mechanical strength, thermal and chemical stability, and exceptional electroisolating properties. In Ref. [61] it was therefore proposed to be used for an EDM experiment. The material absorbs practically no water. Its structure has neither pores nor rough defects or inhomogeneities, thus ensuring a high electric stability. The volume resistivity of our glass ceramics is $\rho > 10^{13}$ Ohmm (20°C). As a special feature one can obtain the compounds with a negative, zero, or even high positive coefficient of thermal expansion, so one can well match contacts with other materials, including metals.

It has been shown experimentally that preliminary baking of the neutron chambers up to ~200°C in vacuum or a helium atmosphere decreases the time needed to raise the high voltage, reduces leakage currents, and enhances the UCN storage lifetime. As the present installation does not permit us to heat the storage chambers *in situ*, baking of components was done periodically in a special box with subsequent reassembly in air, which undoubtedly diminished the effect of heating. The desirable *in situ* baking of the assembled chambers raises several issues. Apart from a more complex setup involving thermal insulation from other parts of the installation, one has to select appropriate materials for the high-voltage electrodes and cylindrical isolators. Gaps between the electrodes and isolators must be minimized to reduce UCN losses, and the components should be made from materials with very similar (or, better, the same) thermal expansion coefficient. For its aforementioned physical properties, glass ceramics might be a suitable choice in future experiments with baking *in situ*. We used glass ceramic rings in our experiments with separate coating and baking in a special oven.

A very important characteristic of the spectrometer is the UCN storage lifetime in the traps. Due to the velocity spectrum of stored neutrons, this cannot be expressed by a single time constant. Within the time interval of holding neutrons in the chamber from 0 to 30 s, the storage lifetime is 30–40 s, whereas for the interval 30–120 s, it is 90–105 s. Figure 6 shows numbers of UCN after different periods of holding them in the top and bottom storage chambers, detected before the spin flipper (Det3, Det4) and after it (Det1, Det2).

A. High-voltage source

A compact bipolar high-voltage supply providing ±200 kV with controlled polarity without using a high-voltage switch

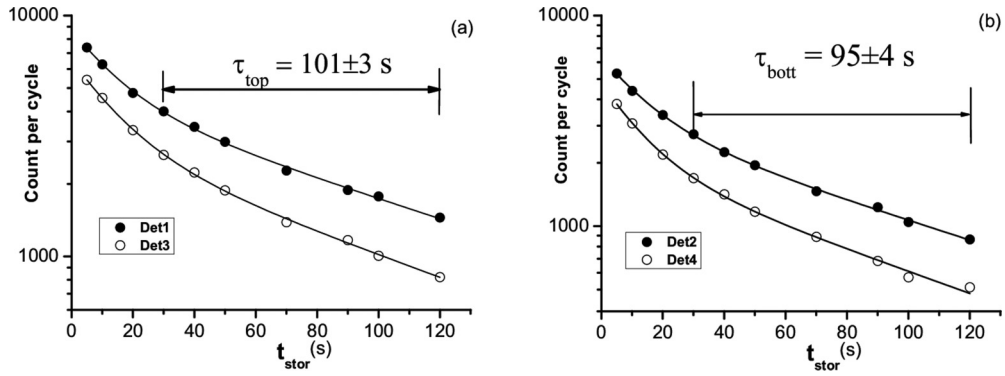

FIG. 6. Measurements of UCN storage in the traps.

was manufactured at PNPI and is similar to an earlier version [62,63]. The source is connected with the spectrometer by means of a 6-m-long HV cable with polyethylene isolation, with the central wire being replaced by distilled water which has a high volume resistivity. The resistance of this cable is 200 MΩ, which, combined with the high internal resistance of the supply, considerably reduces the surges and currents at sparks. High-voltage feedthroughs are made from quartz, with nonvacuum parts within the magnetic screens possessing an additional aluminum cover. To avoid sparks in air gaps of the feedthrough, the space between the cable and an internal surface of the quartz cylinder outside the vacuum chamber is filled with SF_6 to provide insulation. Sparks in the cable and in the feedthrough do not occur until the voltage rises up to ±200 kV and leakage currents do not exceed 1 nA. The HV supply consists of a Cockroft-Walton-type cascade voltage multiplier located in a stainless steel vessel filled with SF_6 at a pressure of 1.5 bars. It also involves a special interface providing controlled reversal of HV polarity at the supply's output without disconnecting the circuit of the load. A flexible design enables operation via manual or computer control. It prohibits simultaneous switching of both polarities of the output voltage and forced reversal of the polarity in case of nonzero output voltage. The main units of the cascade multiplier power module are presented in Fig. 7.

In fact, the cascade multiplier represents two HV stacks of different polarity switched in parallel to a common load. For each HV polarity only one arm serves as HV supply, dependent on which transformer feeds the circuit. Another arm operates as an additional load, serving as a voltage divider on open diodes and resistors. The last resistances of this divider are used for measuring the output voltage. The voltages recorded from both resistive dividers are measured by two separate measuring channels with voltage-to-frequency converters. Simultaneous control of these voltages enables monitoring of internal leakage currents in the HV supply itself (at normal operation these voltages are equal in magnitude but opposite in sign). At reversal of polarity cascade multipliers are swapped, which results in smooth recharging of capacitors of the cascade multipliers without commutation distortions and surge. Figure 8 shows a simplified scheme, and Fig. 9 gives an external view of the cascade multiplier.

The output voltage magnitude, the sign of polarity, and return currents sparks are registered by a PC. For this purpose

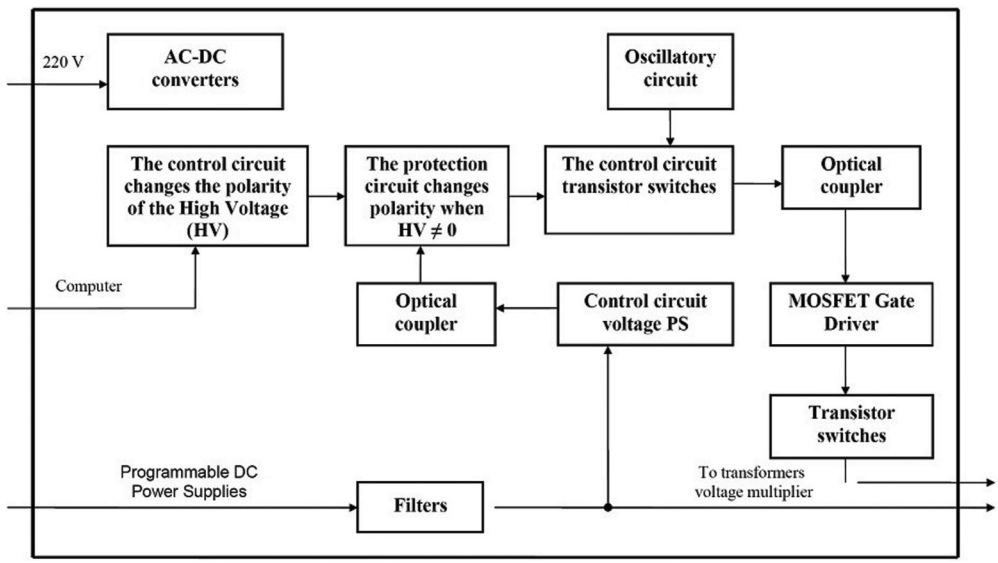

FIG. 7. Block scheme of the power module.

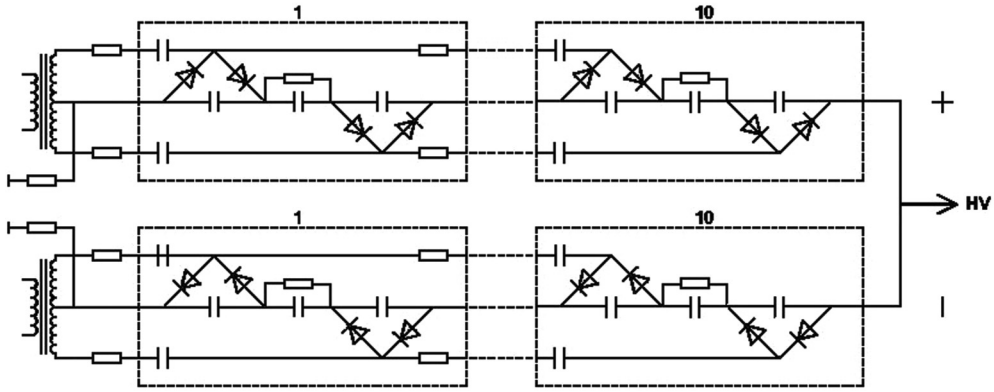

FIG. 8. Layout of the cascade voltage multiplier.

the voltage drops at measuring resistors are converted into frequencies. Data are transmitted by means of fiber optical communication lines, with the measuring facilities being powered by batteries, which provides absence of ground circuits and reduces disturbances. The PC automatically maintains the high voltage value at which the leakage currents do not exceed a preset limit. The system possesses protection from high currents in loads: discharge currents, possible leakage currents in the supply or a short circuit current. The current in loads (one return current for both UCN storage chambers) is measured as voltage drop at an additional resistance of 10 kΩ, in series between the «zero» electrodes and «ground» of the HV supply, using voltage-to-frequency converter. Recording of bipolar pulse signals (caused by the electric discharges at both polarities) is carried out by a single registering channel.

Constant blowing of dry pure helium at pressure $(1-2) \times 10^{-3}$ mbar through the spectrometer permitted us to diminish the total leakage currents of the high-voltage system and increased the operational voltage. Measurements of the neutron EDM thus could be performed at an electric field strength $E = \pm(12-14)\,\mathrm{kV/cm}$, in the best cases even up to 18 kV/cm. The leakage currents in the chambers differed, depending on the quality of the insulator coating, and amounted to values from a few tens up to a few hundreds of nA. At the present accuracy level we have not seen any effect of leakage current on the result of EDM measurement, but for future experiments with significantly improved sensitivity the careful control of leakage currents is crucial.

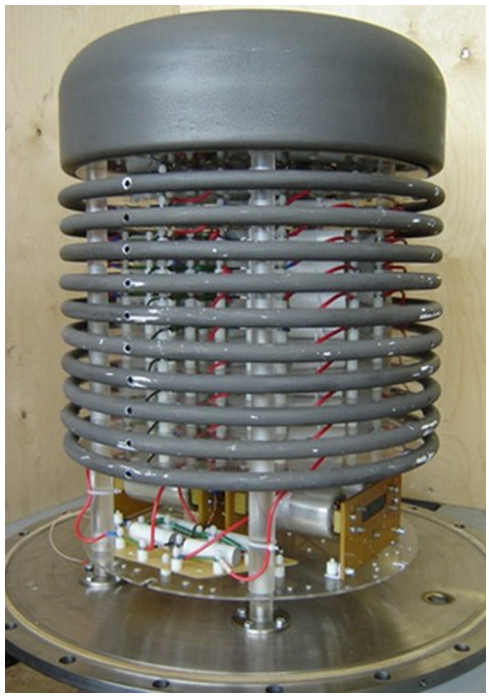

FIG. 9. (Color online) External view on the cascade multiplier.

B. Magnetic fields in the spectrometer

A four-layer magnetic screen made from permalloy protected the spectrometer against outer magnetic perturbations with a dynamic shielding factor of about 1000. For improvement of the magnetic field homogeneity across the neutron chambers, the screens were demagnetized after every dis- and reassembling of the spectrometer. For this purpose an alternating current at frequency of (0.5−1) Hz, with initial amplitude of 20 A was passed through coils for demagnetization and smoothly decreased down to zero (linearly or exponentially) within about 20 min.

A constant and homogeneous magnetic field with strength $B_0 = 1.8 \times 10^{-6}\,\mathrm{T}$ is created in the UCN storage vessels by coils located inside the magnetic screens. The current source feeding these coils has a long-term relative stability of $\sim 10^{-5}$. The oscillating magnetic fields for the rf pulses are induced by a coil consisting of four loops around the UCN storage chambers. The constant and oscillating magnetic fields are thus common for both chambers, while the electric fields have opposite directions in the top and bottom chambers. Trim coils are used for fine corrections of magnetic field homogeneity.

The constant magnetic field is measured by eight cesium magnetometers surrounding the UCN storage chambers. They are placed pairwise in four vertical cylindrical cavity channels fixed on the top of the vacuum chamber. Figure 10 shows a view onto the top lid of the vacuum chamber, with one magnetometer pair removed from its channel. One magnetometer of each pair is located as near as possible to the bottom neutron storage chamber, and the other one to the top chamber. The

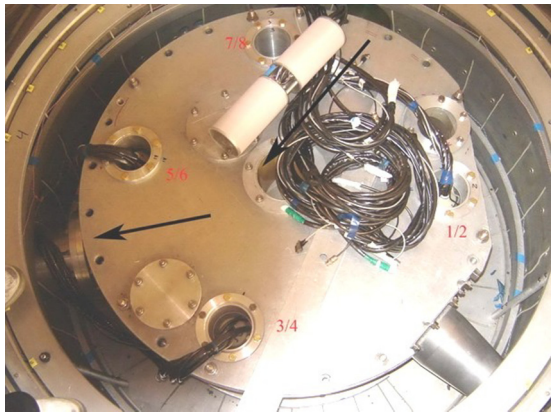

FIG. 10. (Color online) The magnetometer channels of the EDM spectrometer and a dismounted pair of magnetometers. The black cables contain the light guides.

data obtained with these magnetometers are processed by a system of stabilizing neutron magnetic resonance.

Best suited for the stabilization of the resonance is the self-generating mode (of M_x type) based on optical orientation of alkaline atoms [64]. One thus exploits a high sensitivity to magnetic field variations due to a significant atomic polarization and a narrow magnetic-resonance line when using cells with a paraffin coating, as well as a high operating speed peculiar to the M_x circuit. A prototype of the cesium self-generating magnetometer for the EDM experiment [65] demonstrated (in the magnetic field $B_0 = 2 \times 10^{-6}$ T) a sensitivity of $\sim(1-2)$ fT for 100 s integration time. References [66,67] describe the design and implementation of a noise-immune, self-generating cesium magnetometer used here. Figure 11 shows a block diagram of such a magnetometer consisting of a magnetic sensor placed inside the magnetic shield and electronic equipment located outside. The latter features a feedback amplifier and a polarization-pumping light source consisting of a high-frequency (hf) current-stabilized generator, which excites discharges in a cesium spectral lamp. The sensor is coupled to the electronics by three 5-m-long flexible multiple-strand light guides.

The magnetometer operates as follows (see Fig. 11). The light from the Cs spectral lamp passes through light guide, prism, lens, infrared filter ($\lambda_0 = 894.3$ nm), and a circular polarizer. It finally enters into the absorption cell shaped as a glass bulb with an inner paraffin coating and filled with cesium vapors. At magnetic resonance, the light passing through the cell is modulated with the Larmor precession frequency of the Cs atoms. After having passed through another lens, prism, and light guide, the light arrives at a photodetector located on the feedback amplifier board, where it is converted into an alternating current signal amplified by a wideband amplifier with a phase shifter needed for generation. The output voltage of this amplifier varies with the Larmor frequency and controls the luminous power of a light source based on a LED. The modulated light arrives through a light guide at a photodiode connected to the rf coil of the sensor via a capacitor with small leakage (in order to avoid an additional constant magnetic field). As a result, the photodiode converts the modulated light

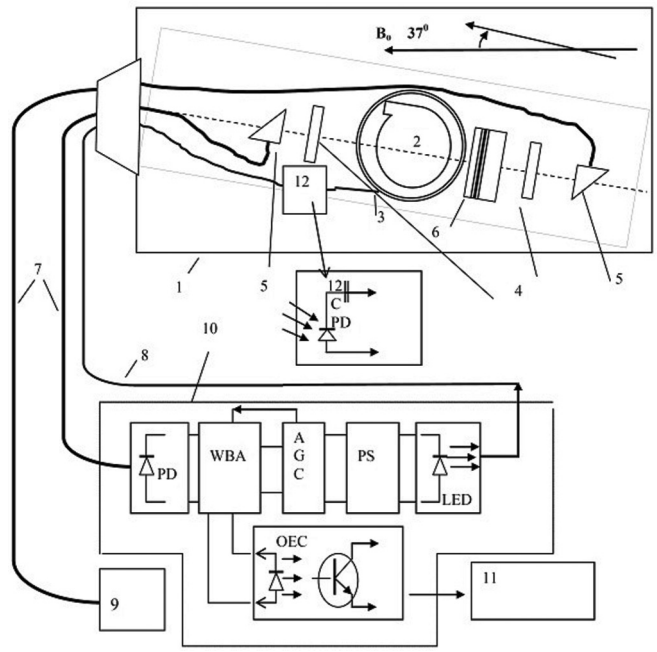

FIG. 11. Block diagram of the noise-immune cesium magnetometer: (1) platform made of Plexiglas; (2) working cell; (3) rf coil; (4) lens; (5) prism; (6) circular polarizer and D1 filter; (7 and 8) light guides; (9) spectral lamp unit; (10) feedback amplifier; (PD) photodiode, (WBA) wideband amplifier, 0.01–2 kHz; (AGC) automatic gain control unit; (PS) phase shifter; (LED) light-emitting diode, part of the optoelectronic device; (OEC) optoelectronic couple; (11) frequency meter; (12) part of the optoelectronic device placed on the magnetometer platform (PD is a photodiode of nonmagnetic design, and C is a blocking capacitor).

into an alternating current, which generates the oscillating magnetic field in the rf coil. Thus, the positive feedback loop is closed. This feedback maintains continuous oscillations in the magnetometer with frequency f proportional to the measured magnetic field $f = B\gamma/2\pi$ (where $\gamma/2\pi = 3.5$ Hz/nT is the gyromagnetic ratio of cesium atoms).

C. Stabilization of the magnetic resonance

Uncontrolled changes of magnetic fields in the UCN storage chambers will lead to resonance frequency shifts, additional spread of the measuring results, and, hence, deterioration of sensitivity. In addition to passive ways of stabilizing the magnetic fields, we use here, as in our previous work [30], a method of active stabilization of the magnetic resonance [68,69], applying modern techniques of digital electronics [70].

The basic idea is as follows. If the frequency f of the oscillating magnetic field $\mathbf{B}_1$ at any time follows any changes of the field $\mathbf{B}_0$, this provides a phase coherence between the oscillating field and the precession of magnetic moments of a neutron ensemble. To obtain a frequency proportional to the mean value of the magnetic field in the neutron storage chambers, one makes use of the mean frequency of the eight quantum self-generating Cs magnetometers surrounding both neutron storage chambers.

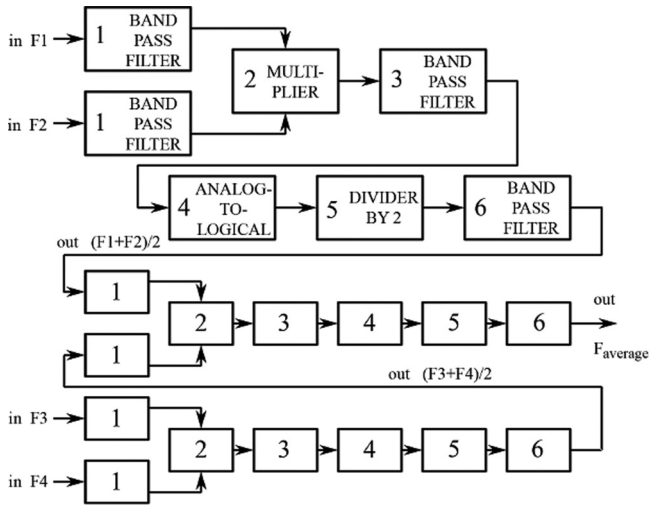

FIG. 12. Block scheme for averaging of frequencies of a quartet of magnetometers.

Since the gyromagnetic ratios for Cs atoms and neutrons differ by a factor 120, the oscillating field $\mathbf{B}_1$ will be close to neutron resonance when dividing the precession frequency of the ^{133}Cs atoms in the field $\mathbf{B}_0$ by this factor. Fast response of the Cs magnetometers provides synchronization of frequency and phases of the rf field pulses $\mathbf{B}_1$ with alterations of $\mathbf{B}_0$.

In the implementation, a digital synthesizer receives an averaged frequency signal (∼6957 Hz) from the eight Cs magnetometers. First, the frequencies from four magnetometers located in the equatorial plane of a neutron chamber are averaged as shown in Fig. 12, separately for the top and the bottom plane. As shown in Fig. 13 the averaged frequencies from each of these two magnetometric quartets are then further averaged. The output frequency of the digital synthesizer of

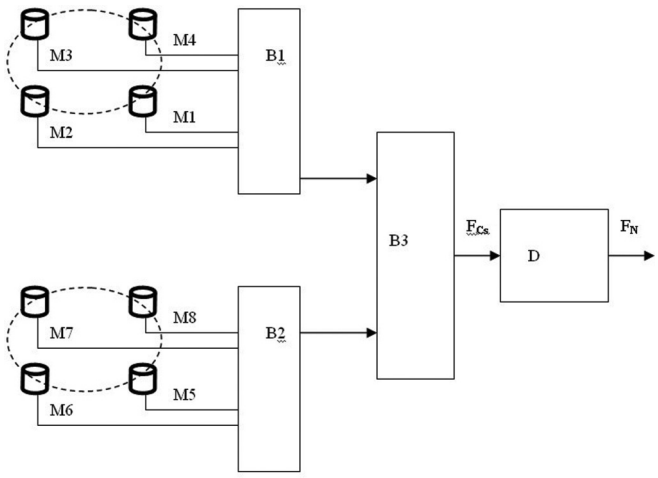

FIG. 13. System for producing the rf field for neutron magnetic resonance. M1–M8: the Cs self-generating magnetometers; B1 and B2: devices for averaging the output frequencies from the Cs magnetometers of the top and bottom neutron chambers, respectively; B3: device for averaging the mean frequencies from B1 and B2; D: digital synthesizer producing the signal for the neutron rf coil.

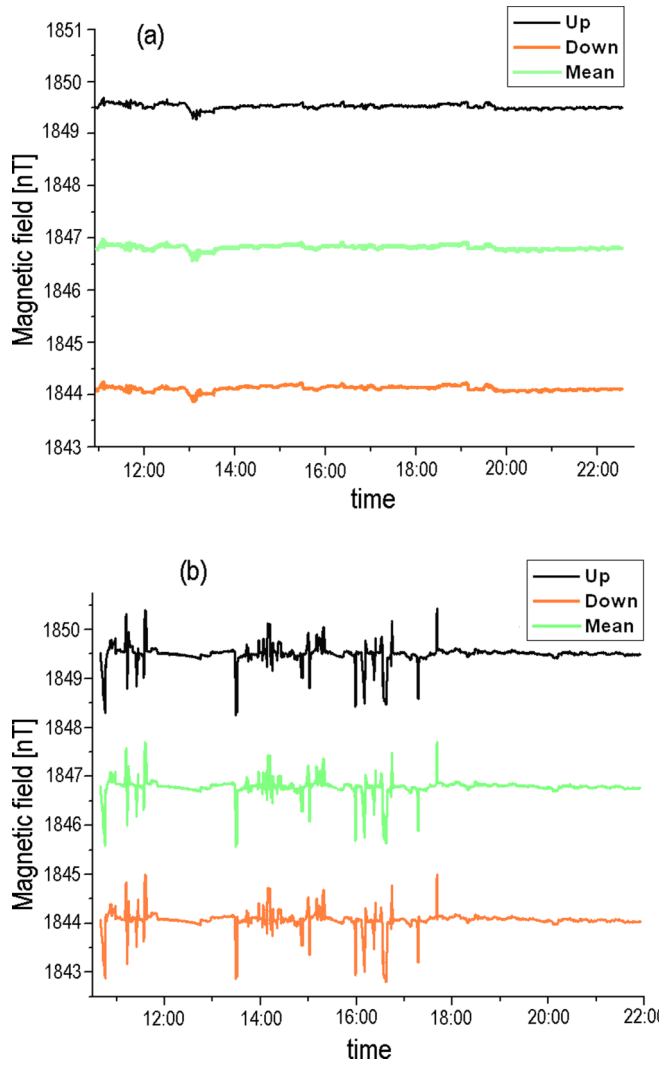

FIG. 14. (Color online) Two examples of magnetic field fluctuations in the spectrometer. Shown are averaged values from the Cs magnetometer close to the upper and the lower neutron chambers, respectively, and the mean value of them. (a) Quite magnetic situation; (b) Noisy magnetic environment caused by bridge-crane movements. Correlated changes of the magnetic field with amplitudes up to 1 nT are observed.

about 58 Hz, used to drive the neutron rf coils, can be varied in steps of 3.3×10^{-6}.

The magnetic field in the spectrometer is influenced by external magnetic perturbations and intrinsic noise. Figure 14 presents two examples of magnetic field behavior: [Fig. 14(a)] quiet magnetic conditions in which measurements were usually made and [Fig. 14(b)] large magnetic perturbations outside the magnetic shield, caused by movement of a bulky bridge crane above the installation. Measurements were not carried on during this period of time. It is noteworthy that the half-width of the neutron resonance after 100 s of free UCN precession corresponds to a magnetic field alteration of only 0.17 nT. Even in quiet magnetic environment, where magnetic field fluctuations inside the shield stay within the half-width of the neutron resonance, stability is not sufficient

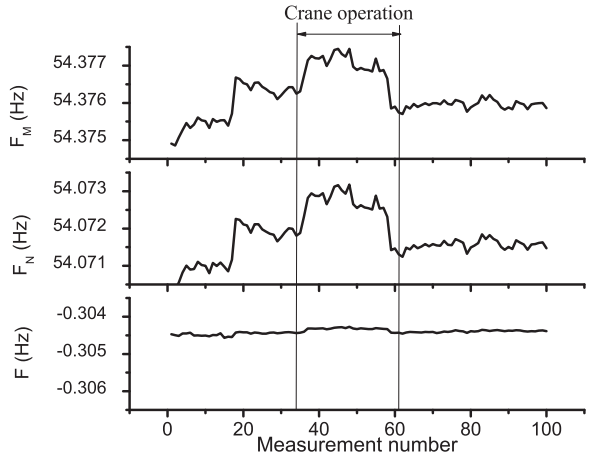

FIG. 15. Mean magnetic field fluctuations in the UCN storage volume area measured by means of Cs magnetometers (see text). The Cs frequency values are quoted after division by the factor 120, i.e., corresponding to the neutron resonance frequency.

for a reliable measurement. Hence, active stabilization of the resonance as described above is of great necessity. Adjustment of the resonances in the top and bottom chambers to the same frequency was achieved by a current in the gradient coils.

The active resonance-stabilization system with its eight Cs magnetometers was tested in a dedicated experiment, performed at relatively small external magnetic field perturbations. The UCN storage chambers were replaced by an additional magnetometer, measuring the field in the center. Figure 15 shows how well the central field (middle plot) corresponds to the mean value calculated from the recordings of the eight Cs magnetometers (upper plot). The difference is shown in the lower plot. As obvious from these figures, active resonance stabilization during neutron EDM measurements will mitigate influences of the external magnetic fluctuations by a factor of 10–15.

Neutron resonance curves, used for the measurement of the slope in the working point as a tool to detect a neutron EDM, were already shown in Fig. 3. They are determined by a variation of the frequency of the rf pulses. In practice, this is obtained by alteration of the frequency division factor within a predetermined range about ∼120, with relative accuracy not lower than 10^{-5}, using the system described above. For compensation of slow changes of the vertical magnetic field gradient and matching of the magnetic resonances in the top and bottom UCN storage chambers, the working points are adjusted via the frequency division factor, using variation of the neutron detector counts, values and signs of the measured derivatives. If resonances deviated by more than 1/4 of a period (corresponding to 0.085 nT for 100 s of UCN storage), the magnetic field gradient was corrected by alteration of current in a gradient coil. Adjustment of the resonances, if necessary, was done only between a series of four measuring cycles (the series is defined in Sec. IV). Using this technique we were able to decrease the spread of measuring results and reduce the final experimental errors practically to the level of statistical spread.

D. Random and systematic errors of the measurements

Magnetic field perturbations in the UCN storage chambers impact the resonance frequency (mitigated by the active compensation described above) and result in an additional spread of experimental data as compared with the Poisson statistics. While external magnetic noises are suppressed to a certain extent by the passive magnetic shield and the active frequency stabilization, likely sources of internal magnetic noise are parasitic currents in the metallic vacuum chamber, in the innermost permalloy screen, and in other conducting components. In order to exclude large closed current loops, all main parts of the installation are isolated from each other and grounded at one point. Another source of disturbances is a magnetic field caused by dis- and recharging currents when switching the electric field in the high voltage circuit. Magnetic field pitches induced by these currents can produce delayed disturbances due to the hysteresis of the magnetic screens.

Variations of magnetic condition in the resonance volume correlated with electric-field reversal result in systematic false effects. They can either distort or imitate a neutron EDM. Correlation data analysis of the multidetector system, leakage currents and magnetometer data recordings, in principle, allows revealing some of them "*a posteriori*." In the sequel such systematic effects are discussed.

$\mathbf{v} \times \mathbf{E}$ *effect*: This most severe systematic effect is due to the magnetic field produced in the frame of the neutron moving through an electric field. According to Lorentz transformation the effective magnetic field (for $\upsilon \ll c$) is given by

$$\mathbf{B}_{\text{eff}} = -\frac{[\mathbf{v} \times \mathbf{E}]}{c^2}.$$

A frequency shift linear in the electric field can arise if the magnetic and electric fields are not parallel. For a small angle ξ between $\mathbf{B}_0$ and $\mathbf{E}$, the magnetic field acquires an additional component parallel to $\mathbf{B}_0$, with sign reversing on reversal of the electric field, and therefore $\Delta B = 2B_{\text{eff}}\xi$. The resonance frequency shift is significantly reduced ($<2 \times 10^{-28} e$ cm) because of the random character of the UCN movement in the chambers. A quadratic effect on the resonance frequency is due to a change of the field modulus even for perfectly aligned electric and magnetic fields, i.e.,

$$B = \sqrt{B_0^2 + B_{\text{eff}}^2} \approx B_0 + \frac{1}{2}\frac{B_{\text{eff}}^2}{B_0}.$$

For an electric field strength of $E = 20\,\text{kV/cm}$ and a UCN velocity of 5 m/s the maximal value of the effective magnetic field corresponds to 100 pT. The total magnetic field alteration due to the quadratic effect is only 2.5 fT, which can imitate EDM value at the level of $4 \times 10^{-27}\, e$ cm. In addition, the impact of this E-field sign-independent effect on the EDM measurement gets further suppressed by a large value when taking differences for electric fields of similar strength but opposite polarities.

Geometric phase: This effect discussed in detail in Ref. [33] occurs due to the Ramsey-Bloch-Siegert shift for particles being stored in a trap with applied $\mathbf{E}$ and $\mathbf{B}_0$ fields. The essence of the effect is that when a gradient $\partial B_{0z}/\partial z$ prevails, UCN detects an additional rotating field $\mathbf{B}_{xy}$ that changes a

precession frequency. The false EDM signal is given by

$$D_{\text{false}} = -\frac{J\hbar}{2}\left(\frac{\partial B_{0z}/\partial z}{B_{0z}^2}\right)\frac{\upsilon_{xy}^2}{c^2}\left[1-\frac{\omega_r^{*2}}{\omega_0^2}\right]^{-1},$$

where $\omega_r^{*2} = \frac{\pi^2}{6}(\frac{\upsilon_{xy}}{R})^2$ and $\upsilon_{xy}^2 = \frac{1}{3}\upsilon_{\max}^2$. Here J is the neutron spin, $\mathbf{v}_{xy}$ is the neutron velocity in the plane perpendicular to $\mathbf{B}_0$, and R is the radius of the neutron storage chamber. Since resonances in upper and bottom chambers are reduced to the same frequency, the average field gradient, affecting the neutrons in the top and bottom storage chambers (with centers separated by 10 cm) does not exceed the value: $\partial B_{0z}/\partial z = 0.85\,\text{nT/m}$. At $B_{0z} = 1.8\,\mu\text{T}$, $\partial B_{0z}/\partial z = 0.85\,\text{nT/m}$, $R = 0.25\,\text{m}$, one obtains: $D_{\text{false}} \leqslant 7.5\times10^{-28}e\text{cm}$.

Leakage currents: The impact on the magnetic resonance depends on the value of these currents and their path over the electrodes and insulators. A difficulty for analysis of EDM data is the lack of knowledge of paths taken by these currents. While in conductors the spatial distribution of leakage currents is predetermined unambiguously, the path over an insulator depends on many factors such as the state of the insulator surface and characteristics of the contact between the insulator and electrode. For an estimate we consider a pessimistic situation for which we evaluate the magnetic resonance shift in terms of the false EDM signal it creates.

The computer modelling of the EDM measurements and the direct calculation of the leakage current effect on the result of measurements were performed.

For the selected path of leakage currents the calculated magnetic field was added to $\mathbf{B}_0$ and the resulting magnetic field was used for calculations of contribution to EDM signal. Large number of possible configurations of the leakage currents was used to make these calculations. The dispersion of the obtained results can serve as an estimation of the leakage current possible

Figure 16 illustrates the distribution of the value of the leakage current influence on the measuring results for two

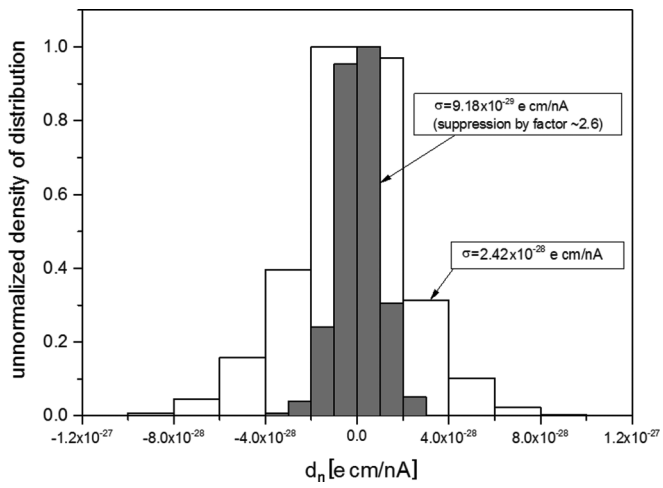

FIG. 16. Distribution of the "measurement" results for random configurations of the leakage currents. The simulated histograms for two independent chambers and for the summary result are given.

TABLE I. Estimates of false signals.

False effect	Estimate
Leakage currents (<100 nA)	$<10^{-26}e$ cm
Square effect $\mathbf{v}\times\mathbf{E}$	$<10^{-28}e$ cm
Nonparallelity of $\mathbf{B}_0$ and $\mathbf{E}$	$<2\times10^{-28}e$ cm
Geometric phase	$<7.5\times10^{-28}e$ cm

chambers if they are independent and for the spectrometer on the whole. One can see that dispersion of results of measurement for the summary result is by ~2.6 times lower than that for separate chambers.

This is concerned with the fact that a leakage current in one chamber also affects the magnetic conditions in another one. Thus, in a differential spectrometer these effects are partially compensated. It can be regarded as another advantage of the double-chamber scheme. The width of the distribution shows a possible false effects when current trajectories are repeated regularly. This is unlikely the case, but the width of the distribution $10^{-28}e\text{cm/nA}$ can be used as upper limit for the false effect. Estimations of the discussed above false signals are presented in Table I.

IV. PROCEDURE OF DATA TAKING, COMPENSATION SCHEME, AND RESULTS OF MEASUREMENTS

A typical cycle of measurements was composed of filling the storage chambers with neutrons for 50 s, UCN storage at constant electric field of defined polarity for 70–100 s, and emptying the storage chambers and detection with polarization analysis for 50 s. To provide the Ramsey-type resonance at the beginning and the end of the storage period, two rf pulses of resonance frequency with duration 3 s and with a relative phase shift of $\pm90^\circ$ were applied.

The HV polarity was reversed within an interval of 50 s between cycles. Four cycles performed in sequence of polarities $+\,-\,-\,+$ or $-\,+\,+\,-$ represent a run of measurements which took about 15 min. This eliminates the effect of linear drifts if measurements are performed within constant time intervals. The alteration of the frequency division coefficient was done between pairs of measuring cycles, so two consecutive cycles with opposite polarity were done with the same division coefficient. These were used for evaluation of the slope (see Sec. II). The phase shift between rf pulses was alternated between 90° or 270° after each run. Correction of resonance, if needed, was performed between the measurement runs.

In order to perform measurements of EDM values d_i one first has to determine the working point where the frequencies of Larmor precession and the rf field are exactly the same. This is done with measurements for different time intervals T between rf pulses, the working point being independent of duration of intervals. Highest sensitivity to the neutron EDM is achieved if one applies phase shifts $\Delta\phi$ of 90° or 270° between the two rf pulses. As shown in Fig. 3 this leads to the steepest slope $\partial N/\partial f$ of neutron counts at the

working point [compare with Eq. (2)]. For each of the two phase shift settings the slope is determined from two neutron count rates obtained with small shifts of the radio frequency by about $\Delta f = \pm 5 \times 10^{-4}$ Hz around the working point. Experimental evaluation of magnitude and sign of the slope allows us to control a drift of the working point during the measurement which adjusted automatically in case of a drift of the resonance. This provides an additional stabilization of the resonance.

From the count rates of all four detectors D_1-D_4 (see Fig. 4) we can obtain values $d_1, \ldots, d_4$ for the neutron EDM using Eq. (1). Compensation, respectively, determination of some systematic effects is obtained by using linear combinations of them:

$$
\begin{aligned}
\mathrm{EDM} &= \frac{1}{4}[(d_1 + d_2) + (d_3 + d_4)] = \frac{1}{4}\frac{h}{2(E^+ + E^-)}[(\Delta\nu_1 - \Delta\nu_2) + (\Delta\nu_3 - \Delta\nu_4)] \\
&= \frac{1}{4}\frac{h}{2(E^+ + E^-)}\frac{1}{\partial N/\partial f}[(\Delta N_1 - \Delta N_2) - (\Delta N_3 - \Delta N_4)] \\
\Delta\nu &= \frac{1}{4}[(d_1 - d_2) + (d_3 - d_4)] = \frac{1}{4}\frac{h}{2(E^+ + E^-)}(\Delta\nu_1 + \Delta\nu_2 + \Delta\nu_3 + \Delta\nu_4) \\
&= \frac{1}{4}\frac{h}{2(E^+ + E^-)}\frac{1}{\partial N/\partial f}[(\Delta N_1 + \Delta N_2) - (\Delta N_3 + \Delta N_4)] \\
\Delta N &= \frac{1}{4}[(d_1 - d_2) - (d_3 - d_4)] = \frac{1}{4}\frac{h}{2(E^+ + E^-)}[(\Delta\nu_1 + \Delta\nu_2) - (\Delta\nu_3 + \Delta\nu_4)] \\
&= \frac{1}{4}\frac{h}{2(E^+ + E^-)}\frac{1}{\partial N/\partial f}(\Delta N_1 + \Delta N_2 + \Delta N_3 + \Delta N_4) \\
Z &= \frac{1}{4}[(d_1 + d_2) - (d_3 + d_4)] = \frac{1}{4}\frac{h}{2(E^+ + E^-)}[(\Delta\nu_1 - \Delta\nu_2) - (\Delta\nu_3 - \Delta\nu_4)] \\
&= \frac{1}{4}\frac{h}{2(E^+ + E^-)}\frac{1}{\partial N/\partial f}[(\Delta N_1 - \Delta N_2) + (\Delta N_3 - \Delta N_4)]. \qquad (3)
\end{aligned}
$$

The first equation determines a value for the neutron EDM. For a fully symmetric setup, this combination of values d_i completely compensates fluctuations common to both chambers and correlated with reversal of the electric fields. Moreover, the linearly independent second and third combinations in Eq. (3) provide measurements of such fluctuations and hence control over systematic effects. While $\Delta\nu$ is sensitive to electric-field influences on the resonance conditions, ΔN measures a systematic effect on neutron count rates. Finally, in the last combination Z all aforementioned effects (including the neutron EDM) are compensated, so the condition $Z = 0$ provides a crucial test of the compensation scheme.

Note that this scheme is able to compensate an effect on $\Delta\nu$, in case of homogeneous changes of magnetic fields correlated with HV switching. The same is true for ΔN, in case of a similar influence on all electronic circuits of counters, for which a large degree of compensation is not to be expected. One should take into consideration the appearance of a statistically meaningful signal (over 3–4 standard deviations), find the reasons, and take measures for their elimination. As shown before, active compensation suppresses homogenous magnetic perturbations by approximately 10–15 times (see Fig. 15).

We also note that if there is an influence of the electric field switching on neutron-detection equipment (effect ΔN caused by electromagnetic disturbances, stray pickups, etc.), then it should not depend on the phase of the resonance curve. Therefore, to correctly identify this effect, the magnitudes ΔN in Eq. (3) for $\Delta\varphi = 90^\circ$ and $\Delta\phi = 270^\circ$ need to be subtracted, but not summed, because they are obtained for the resonance curves with slopes of opposite sign.

The measurements were carried out at the ultracold neutron facility PF2 at the ILL. As determined in prior experiments the beam port PF2-MAM provides a UCN number density of about 7.5 n/cm^3 at the entrance of the EDM spectrometer [59]. Figure 17 presents an exemplary series of experimental data taken during 15 h, with an electric field of 18 kV/cm, and

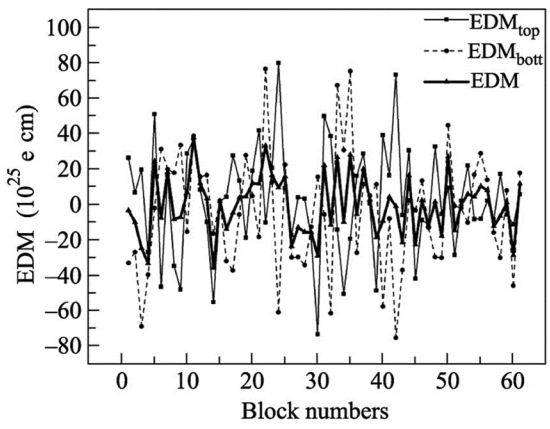

FIG. 17. Exemplary series of measurements. $\mathrm{EDM_{top}}$ and $\mathrm{EDM_{bott}}$ are values measured for the top and bottom chambers separately (see text). EDM is the quantity defined in Eq. (3) providing the neutron EDM using measurements with both chambers and all four UCN detectors.

TABLE II. Results of measurements in units of $10^{-26}e$ cm.

	Previous (PNPI) [30]	New (ILL) [36]	Total
EDM	0.7 ± 4.0	0.36 ± 4.68	0.56 ± 3.04
$\Delta\nu$	-22.8 ± 9.2	-10.04 ± 5.98	-13.8 ± 5.01
ΔN	-14.5 ± 4.4	18.62 ± 5.15	-0.53 ± 3.35
Z	-0.8 ± 4.0	3.68 ± 4.72	1.05 ± 3.05

a UCN storage time of 100 s. Each point represents the result of a single measurement sequence of the value of EDM in accordance with Eqs. (1) and (3). Also quoted are separate results on the quantities $\mathrm{EDM_{top}} = (d_1 + d_3)/2$ and $\mathrm{EDM_{bott}} = (d_2 + d_4)/2$ for the top and bottom chambers separately. Total results from the series shown in Fig. 17 are $\mathrm{EDM_{top}} = (2.59 \pm 3.90) \times 10^{-25} e\mathrm{cm}$, $\mathrm{EDM_{bott}} = -(3.98 \pm 4.22) \times 10^{-25} e\mathrm{cm}$, and $\mathrm{EDM} = -(0.70 \pm 2.17) \times 10^{-25} e\mathrm{cm}$. The latter permits us to assess the sensitivity of the experiment when running under smooth conditions, which for this series of measurements amounted to $1.7 \times 10^{-25} e\mathrm{cm/day}$.

The measurements were conducted in series during three reactor cycles of 50 days each. The duration of a series of continuous measurements depended on the magnetic field fluctuations in the experimental hall. At large magnetic fluctuations, the measurements had to be stopped, and then it was necessary to retune the spectrometer and bring the magnetic resonances of the top and bottom UCN storage chambers back to coincidence. This led to a significant loss of time. Another important reason for time loss was waiting for the beam shared with several other UCN users at other positions of the UCN turbine. In August 2013 the reactor was shut down for a scheduled long-term preventive maintenance and upgrade. The results for EDM, $\Delta\nu$, ΔN, and Z in units of $10^{-26} e\mathrm{cm}$ are listed in the Table II along with the data obtained earlier at the same EDM spectrometer at PNPI [30]. The difference from zero for the EDM and Z quantities does not exceed one standard deviation in all measurements. The $\Delta\nu$ and ΔN quantities, on the other hand, deviate from zero by 2 and 3.5 standard deviations, respectively, the latter with different signs in the two measurements. The last column of Table II shows overall results obtained using this spectrometer at PNPI and ILL.

Since the crucial criterion $Z = 0$ is fulfilled, we assume systematic effects to be visible in $\Delta\nu$ and ΔN as compensated in the value of EDM. As mentioned above, our spectrometer scheme can compensate homogenous changes, while the inhomogeneous fluctuations of magnetic field resulting from the leakage currents cannot be fully compensated. Therefore, special attention must be paid to analyze data depending on the leakage currents. During data taking at various times the leakage currents were differed and usually ranged from a few tens up to a few hundreds of nA and never exceeded 2000 nA.

To test the possible influence of leakage currents on the values of EDM, $\Delta\nu$, ΔN, and Z, series were grouped on the basis of a mean value of the leakage currents measured during neutron storage. Current ranges of the groups were chosen as follows: 0–50 nA, 50–100 nA, 100–150 nA, 150–300 nA, 300–500 nA, 500–1000 nA, and 1000–2000 nA. The results

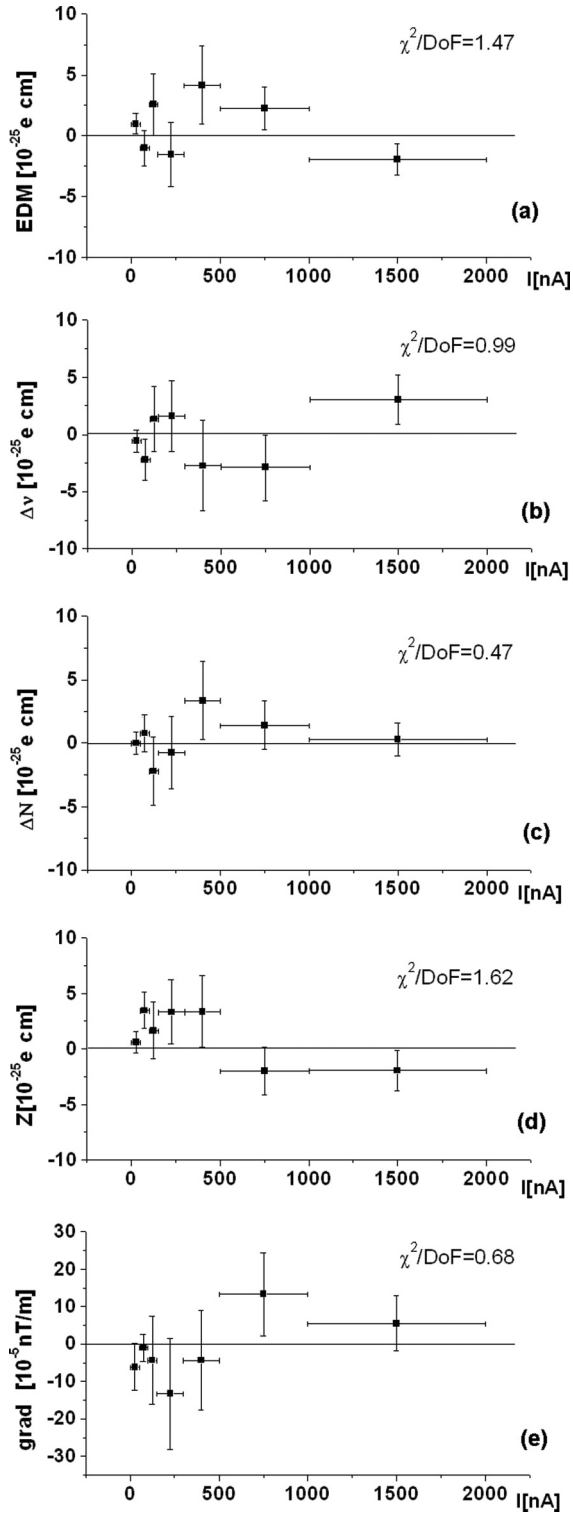

FIG. 18. Results of measurements of the various quantities given in Eq. (3) for different ranges of leakage current. For explanation of the lowest plot see text.

are given in Fig. 18. The quoted χ^2 values characterize the spread of data for the hypothesis of a zero average.

As nonidentical changes of a magnetic field in the top and bottom neutron storage chambers are not compensated

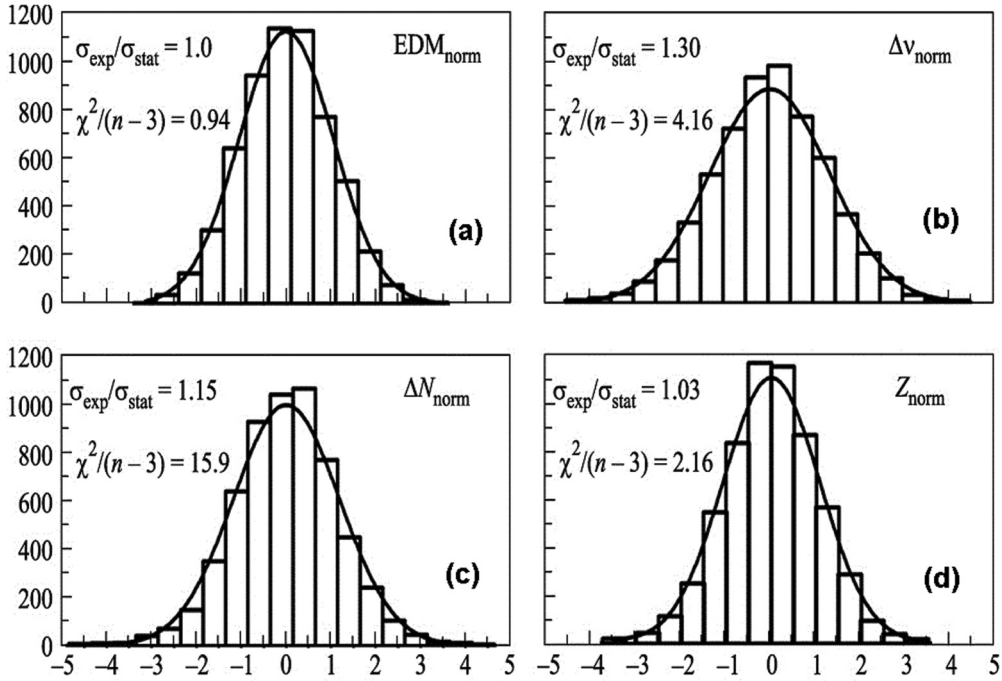

FIG. 19. Distribution of measured values for the quantities defined in Eq. (3). For each quantity is shown the ratio of the width of the measured values distribution to its uncertainty defined by counting statistics, as well as χ^2 obtained from fitting a normal distribution.

by a differential spectrometer, the lowest plot shows magnetic field gradient values, measured in the same time intervals as a function of leakage current. The gradient is calculated from the difference between the average values of magnetic fields measured by the upper and the lower magnetometers during neutron storage. No dependence on leakage current is observed in any of the quantities.

A separate control of the cesium magnetometers has shown that after electric-field reversal the difference in magnetometer readings in the upper and lower planes (see Fig. 4) did not exceed 1 fT, as determined with all data accumulated during the EDM measurements. This represents a corresponding false EDM signal below $2 \times 10^{-27} e$cm, i.e., by still more than a factor 10 beyond the quoted accuracy of the EDM measurements.

Distributions of measured normalized values of EDM, $\Delta\nu$, ΔN, and Z are presented in Fig. 19 (normalized values are $Y_i = (y_i - \langle y \rangle)/\sigma$, where y_i are measured values, $\langle y \rangle$ is the mean value, and σ is the standard deviation).

The width of the distributions of EDM and Z values corresponds to that of a normal distribution defined by counting statistics. The distributions of values of $\Delta\nu$ and ΔN are somewhat broadened due to imperfect stability of the magnetic field and fluctuations of neutron counts. The absence of any additional broadening of the EDM and Z distributions demonstrates the compensation of magnetic field fluctuations.

The accuracy of the reported measurements of neutron EDM at ILL was $4.7 \times 10^{-26} e$cm. Including the earlier result obtained at the WWR-M reactor at PNPI [30] the total accuracy is $3.0 \times 10^{-26} e$cm. We interpret our new result as a limit on the neutron electric dipole moment of $|d_n| < 5.5 \times 10^{-26} e$cm at 90% confidence level. This result is slightly weaker than the result $2.9 \times 10^{-26} e$ cm [32]. However, it was obtained in an independent experiment using a setup offering experimental control over false signals as a strong asset for a reliable measurement.

V. POSSIBILITIES FOR ENHANCING THE EXPERIMENTAL PRECISION

The sensitivity of our spectrometer and the resulting accuracy of measurements were limited mainly by the number of registered neutrons. In the best series of measurements reported here, the sensitivity of the EDM spectrometer was $\delta d_n = 1.7 \times 10^{-25} e$cm per day. This shall be improved by relocation of the spectrometer to another UCN beam at PF2, with 3–4 times higher intensity than at PF2/MAM [59]. In addition, an upgrade of the spectrometer is in progress, involving filling and emptying of the storage chambers via the central electrode. This will enable us to get rid of some parts of the neutron guides with small bending radius and thus to decrease some neutron losses. We are also working on improving other parameters of the spectrometer: the UCN storage time constant, neutron polarization and a stronger electric field in the UCN storage chambers. Thereby, a statistical accuracy of the EDM value of $10^{-26} e$cm should become possible within 100 days of measurements.

Further prospects for the EDM experiment will require creation of a new generation of UCN sources such as the project SuperSUN at ILL [71] prepared in prototyping stages [44,45], or the source to be built at PNPI for a new reactor PIK with a prototype under construction at the WWR-M reactor at PNPI [58], all employing converters of superfluid He. At the latter source one may expect to obtain UCN densities up to $10^4 \mathrm{UCN/cm^3}$. This implies that the spectrometer will have to

comply with far more stringent quality requirements in order to enable measurements of the neutron EDM at the accuracy level better than $10^{-27}e$ cm.

ACKNOWLEDGMENTS

We are grateful to the staff of the workshop of experimental facilities at PNPI for their assistance in reconstructing the spectrometer and to the personnel of the ILL reactor for help in assembling the installation and assistance during the data taking. We thank T. Brenner from ILL and A. I. Egorov, E. P. Volkov, E. V. Siber, A. A. Sumbatian, and T. V. Savelieva from PNPI for their assistance. We also acknowledge a large contribution from I. Tokmakov, N. Mikulinas, and A. Pikalev on the development and construction of the high-voltage source.

Various parts of the carried out research was executed at the PNPI NRC "Kurchatov Institute" with support of the Russian Foundation for Basic Research (Project No. 14-02-00051) and the Russian Science Foundation (Project No. 14-22-00105) in full conformity with the independent plans of these projects.

[1] E. M. Purcell and N. F. Ramsey, Phys. Rev. **78**, 807 (1950).
[2] J. H. Smith, E. M. Purcell, and N. F. Ramsey, Phys. Rev. **108**, 120 (1957).
[3] T. D. Lee and C. N. Yang, Phys. Rev. **104**, 254 (1956).
[4] C. S. Wu, E. Ambler, R. W. Hayward, D. D. Hoppes, and R. P. Hudson, Phys. Rev. **105**, 1413 (1957).
[5] J. H. Christenson, J. W. Cronin, V. L. Fitch, and L. Turlay, Phys. Rev. Lett. **13**, 138 (1964).
[6] L. Canetti, M. Drewes, and M. Shaposhnikov, New J. Phys. **14**, 095012 (2012).
[7] P. Huet and E. Sather, Phys. Rev. D **51**, 379 (1995).
[8] X.-G. He, B. H. J. McKellar, and S. Pakvasa, Int. J. Mod. Phys. A **4**, 5011 (1989).
[9] I. Bigi and N. G. Ural'tsev, Zh. Eksp. Teor. Fiz. **100**, 363 (1991) [Sov. Phys. JETP **73**, 198 (1991)].
[10] M. Pospelov and A. Ritz, Ann. Phys. **318**, 119 (2005).
[11] J. Engel, M. J. Ramsey-Musolf, and U. van Kolck, Prog. Part. Nucl. Phys. **71**, 21 (2013).
[12] T. Chupp, M. Ramsey-Musolf, Phys. Rev. C **91**, 035502 (2015).
[13] J. Baron, W. C. Campbell, D. DeMille *et al.*, Science **343**, 269 (2014).
[14] M. J. Ramsey-Musolf (private communication).
[15] V. Cirigliano, Y. Li, S. Profumo, and M. J. Ramsey-Musolf, J. High Energy Phys. 01 (2010) 002
[16] W. B. Dress, P. D. Miller, J. M. Pendlebury, P. Perrin, and N. F. Ramsey, Phys. Rev. D **15**, 9 (1977).
[17] C. Shull and R. Nathans, Phys. Rev. Lett. **19**, 384 (1967).
[18] V. L. Alekseev, V. V. Voronin, E. G. Lapin *et al.*, Zh. Eksp. Teor. Fiz. **96**, 1921 (1989) [Sov. Phys. JETP **69**, 1083 (1989)].
[19] V. V. Fedorov, V. V. Voronin, and E. G. Lapin, J. Phys. G: Nucl. Part. Phys. **18**, 1133 (1992).
[20] V. V. Fedorov, M. Jentschel, I. A. Kuznetsov *et al.*, Phys. Lett. B **694**, 22 (2010).
[21] Ya. B. Zel'dovich, Zh. Eksp. Teor. Fiz. **36**, 1952 (1959) [Sov. Phys. JETP **9**, 1389 (1959)].
[22] F. L. Shapiro, Usp. Fiz. Nauk **95**, 145 (1968) [Sov. Phys. Usp. **11**, 345 (1968)].
[23] V. I. Lushchikov, Yu. N. Pokotilovskii, A. V. Strelkov, and F. L. Shapiro, Pis'ma Zh. Eksp. Teor. Fiz. **9**, 40 (1969) [Sov. Phys. JETP Lett. **9**, 23 (1969)].
[24] A. Steyerl, Phys. Lett. B **29**, 33 (1969).
[25] I. S. Altarev *et al.*, Nucl. Phys. A **341**, 269 (1980).
[26] I. S. Altarev *et al.*, Phys. Lett. B **102**, 13 (1981).
[27] J. M Pendlebury *et al.*, Phys. Lett. B **136**, 327 (1984).
[28] K. F. Smith *et al.*, Phys. Lett. B **234**, 191 (1990).
[29] I. S. Altarev *et al.*, Phys. Lett. B **276**242 (1992).
[30] I. S. Altarev, Yu. V. Borisov, N. V. Borovikova *et al.*, Yad. Fiz. **59**, 1204 (1996) [Phys. At. Nucl. **59**, 1152 (1996)].
[31] P. G. Harris *et al.*, Phys. Rev. Lett. **82**, 904 (1999).
[32] C. A. Baker, D. D. Doyle, P. Geltenbort *et al.*, Phys. Rev. Lett. **97**, 131801 (2006).
[33] J. M. Pendlebury *et al.*, Phys. Rev. A **70**, 032102 (2004).
[34] I. S. Altarev, N. V. Borovikova *et al.*, Pis'ma Zh. Eksp. Teor. Fiz. **44**, 269 (1986) [JETP Lett. **44**, 344 (1986)].
[35] A. Steyerl, H. Nagel *et al.*, Phys. Lett. A **116**, 347 (1986).
[36] A. P. Serebrov, E. A. Kolomenskiy, A. N. Pirozhkov *et al.*, JETP Lett. **99**, 4 (2014).
[37] I. Altarev, D. H. Beck, S. Chesnevskaya *et al.*, Nuovo Cimento C **35**, 122 (2012).
[38] C. Baker, G. Ban, K. Bodek *et al.*, Phys. Proc. **17**, 159 (2011).
[39] Y. Masuda, K. Asahi, K. Hatanaka *et al.*, Phys. Lett. A **376**, 1347 (2012).
[40] The EDM@SNS neutron EDM experiment, http://p25ext.lanl.gov/edm/edm.html.
[41] R. Golub and S. K. Lamoreaux, Phys. Rep. **237**, 1 (1994).
[42] F. M. Piegsa, Phys. Rev. C **88**, 045502 (2013).
[43] M. G. D. van der Grinten, Nucl. Instrum. Methods A **611**, 129 (2009).
[44] F. M. Piegsa, M. Fertl, S. N. Ivanov *et al.*, Phys. Rev. C **90**, 015501 (2014).
[45] O. Zimmer, F. M. Piegsa, and S. N. Ivanov, Phys. Rev. Lett. **107**, 134801 (2011).
[46] A. Saunders, M. Makela, Y. Bagdasarova *et al.*, Rev. Sci. Instrum. **84**, 013304 (2013).
[47] B. Lauss, Phys. Procedia **51**, 98 (2014).
[48] U. Trinks, F. J. Hartmann, S. Paul, and W. Schott, Nucl. Instrum. Methods A **440**, 666 (2000).
[49] O. Zimmer, K. Baumann, M. Fertl *et al.*, Phys. Rev. Lett. **99**, 104801 (2007).
[50] O. Zimmer, P. Schmidt-Wellenburg, M. Fertl *et al.*, Eur. Phys. J. C **67**, 589 (2010).
[51] A. Frei, Y. Sobolev, I. Altarev *et al.*, Eur. Phys. J. A **34**, 119 (2007).
[52] T. Lauer and T. Zechlau, Eur. Phys. J. A **49**, 104 (2013).
[53] J. Karch, Yu. Sobolev, M. Beck *et al.*, Eur. Phys. J. A **50**, 78 (2014).
[54] Y. Masuda, T. Kitagaki, K. Hatanaka *et al.*, Phys. Rev. Lett. **89**, 284801 (2002).

[55] Y. Masuda, K. Hatanaka, S.-C. Jeong *et al.*, Phys. Rev. Lett. **108**, 134801 (2012).
[56] E. I. Korobkina, B. W. Wehring, A. I. Hawari *et al.*, Nucl. Instrum. Methods A **579**, 530 (2007).
[57] A. P. Serebrov, A. K. Fomin, M. S. Onegin *et al.*, Tech. Phys. Lett. **40**, 10 (2014).
[58] A. P. Serebrov, V. A. Mityuklyaev, A. A. Zakharov *et al.*, Nucl. Instrum. Methods A **611**, 276 (2009).
[59] A. P. Serebrov, P. Geltenbort, I. V. Shoka *et al.*, Nucl. Instrum. Methods A **611**, 263 (2009).
[60] N. F. Ramsey, *Molecular Beams* (Oxford University Press, New York, 1956).
[61] I. S. Altarev, Yu. V. Borisov, S. N. Ivanov *et al.* (unpublished).
[62] Yu. V. Borisov, USSR Inventor's Certificate no. 944021 (1980). Byull. Izobret., 1982, no. 26.
[63] Yu. V. Borisov *et al.*, Prib. Tekh. Eksp. **2**, 120 (1987) [Instrum. Exp. Tech. **30**, 376 (1987)].
[64] N. M. Pomerantsev, V. M. Ryzhkov, and G. V. Skrotskii, *Fizicheskie osnovy kvantovoi magnitometrii (Physical Bases of Quantum Magnetometry)* (Nauka, Moscow, 1972).
[65] E. B. Aleksandrov, M. V. Balabas, S. P. Dmitriev *et al.*, Tech. Phys. Lett. **32**, 627 (2006).
[66] Yu. V. Borisov and V. N. Slyusar', USSR Inventor's Certificate no. 1691804, Byull. Izobret., 1991, no. 42, p. 15.
[67] E. B. Aleksandrov, M. V. Balabas, Yu. V. Borisov *et al.*, Instrum. Exp. Tech. **50**, 91 (2007).
[68] Yu. V Borisov and S. N. Ivanov, USSR Inventor's Certificate no. 919477, Byull. Izobret., 1983, no. 30.
[69] Yu. V. Borisov, S. N. Ivanov, V. M. Lobashev *et al.*, Nucl. Instrum. Methods A **357**, 115 (1995).
[70] E. B. Aleksandrov, M. V. Balabas, Yu. V. Borisov *et al.*, Tech. Phys. Lett. **33**, 3 (2007).
[71] O. Zimmer, R. Golub, Phys. Rev. C **92**, 015501 (2015).